Abnormal elemental redistribution in oxyfluoride glasses induced by high repetition rate femtosecond laser

Shengzhi Sun (孙盛芝)[1], Song Ye (叶 松)[2], Zhenyan Wang (王振彦)[1], Juan Song (宋 娟)[3], Bin Qian (钱 滨)[4,*], and Jianrong Qiu (邱建荣)[4,]**

[1]*Ningbo University of Finance and Economics, Ningbo 315175, China*
[2]*School of Materials Science and Engineering, Tongji University, Shanghai 201804, China*
[3]*School of Material Science and Engineering, Jiangsu University, Zhenjiang 212013, China*
[4]*State Key Laboratory of Modern Optical Instrumentation, College of Optical Science and Engineering, Zhejiang University, Hangzhou 310027, China*
**Corresponding author: binqian1984@163.com; **corresponding author: qjr@zju.edu.cn*
Received January 15, 2019; accepted March 28, 2019; posted online June 11, 2019

We report on the elemental redistribution behavior in oxyfluoride glasses with a high repetition rate near-infrared femtosecond laser. Elemental analysis by an electro-probe microanalyzer demonstrates that the redistributions of Ca^{2+} and Yb^{3+} ions change dramatically with pulse energy, which are quite different compared with previous reported results. Confocal fluorescence spectra of Yb^{3+} ions demonstrate that the luminescence intensity changes obviously with the elemental redistribution. The mechanism of the observed phenomenon is discussed. This observation may have potential applications in the fabrication of micro-optical devices.
OCIS codes: 160.5690, 160.2750, 160.4760, 350.3390.
doi: 10.3788/COL201917.061601.

Femtosecond (fs)–laser-induced micro-modifications in transparent materials have attracted considerable interest and been extensively studied for several decades[1–3]. Owing to its unique advantages (high accuracy, low thermal effect, and minimum collateral damage), fs laser micromachining is considered and confirmed as one of the most promising ways to modify the micro-properties of transparent materials, such as glasses[2,4–6], crystals[3,7], and polymers[8]. With fs lasers, various micro-properties of materials can be modified, for instance, conversion of single crystal, polycrystal, and amorphous[9,10], modification of refractive index[11], change of valence state[12,13], precipitation of nanoparticles[14,15], and selective migration of ions[16]. All these changes induced by a fs laser can be used for fabrication of functional micro-optical devices, such as optical waveguides[17], directional couplers[18], three-dimensional (3D) optical data storage media[19], and 3D micro-fluidic devices[20,21].

Recently, space-selective manipulation of elements in glass by a fs laser has been an advanced research hotspot[16,22], since most optical properties of materials such as absorption, luminescence, refractive index, and optical nonlinearity are highly related to element distribution. Numerous interesting phenomena as well as potential applications have been reported by several research groups[16,23–30]. Microscopic control of the intensity distribution of luminescence[23] and simultaneous control over the precipitation of multiple crystalline phases and active ion migration[27] have been realized in some materials. Furthermore, a method for controlling the shape of the elemental distribution with a spatial light modulator has been reported[28]. According to previous observation[2,23–25], the relative concentration of glass network modifying ions is usually higher at the periphery and lower in the central area of the laser-affected region, indicating that the network modifying ions tend to diffuse from the vicinity of the focal point to the boundary of the laser modified area. Meanwhile, the relative concentration of glass network forming ions is opposite to that of network modifying ions, migrating from the periphery of the modified region to the center. Generally, diffusion coefficients of different elements and temperature gradients are considered to be the key factors for the formation mechanism of element migration[16,29]. However, a few experiment results that do not conform with the previous proposition mentioned above have also been reported[31,32], demonstrating that the mechanism of element migration might be more complicated than what was previously proposed.

In this Letter, we report on an abnormal phenomenon of element migration in oxyfluoride glasses after the irradiation of a 250 kHz fs laser at 800 nm. Electron microprobe analysis shows that the distributions of elements (Ca^{2+}, Yb^{3+}, and Si^{4+}) are highly dependent on laser pulse energy. The glass network modifying ions (Ca^{2+} and Yb^{3+}) migrate to the center area at lower pulse energy, while they diffuse to the periphery of the modified region at higher pulse energy. The possible mechanism for this diversified migration of elements has been discussed, including the influences of temperature gradient, diffusion coefficient, and laser-induced crystallization. Moreover, the relationship between element distribution and fluorescence intensity of Yb^{3+}has been investigated with the confocal fluorescence spectrum, indicating that space-selective manipulation of element distribution is a promising way to fabricate multifunctional optical devices in glasses.

In this work, a glass with the composition of $60SiO_2$–$20Al_2O_3$–$20CaF_2$–$6YbF_3$–$0.2TbF_3$ (mol%) was chosen for the study. The raw materials (high purity SiO_2, Al_2O_3, CaF_2, TbF_3, and YbF_3) were mixed thoroughly and melted in a covered corundum crucible at 1400°C for 30 min in air. The melt was then cast onto a steel plate and quenched quickly with another plate. The samples were cut and six-facet polished into 5 mm × 5 mm × 2 mm dimensions for the irradiation experiments.

A high repetition rate fs laser (HRRFS) was employed as the laser source, which emits 800 nm, 70 fs, and 250 kHz mode-locked pulses. The laser beam was focused via a 50× objective lens (numerical aperture = 0.8) into the glass sample. The glass sample was put on an *XYZ* motorized stage with its top facet perpendicular to the laser beam, as shown in Fig. 1. Laser processed lines vertical to the surface of the glass sample were written inside the glass sample with a length of 1.5 mm, using sample translation in the vertical (*Z*) direction at the speed of 6 μm/s. The pulse energy was varied from 2.0 up to 3.52 mJ. After irradiation, the glass sample was cut along the plane perpendicular to the written lines and polished to optical quality so as to expose the cross sections of the laser processed lines for elemental analysis. The elemental distribution of the ions around the focal point in the glass sample was characterized with an electro-probe microanalyzer (EPMA, JEOL, model JSM-6700F). We confirmed that there was no apparent change in the element distribution along the *Z* direction. The confocal fluorescence spectra were measured by a Raman spectrometer (JOBLN-YVON, T6400) with a 785 nm laser excitation.

To determine the element distribution in the laser-affected zone, the EPMA measurement was performed on the samples. Figure 2 shows the relative concentration of glass modifier Ca^{2+} and Yb^{3+} ions in the laser modified region with different pulse energy.

It is obvious that the migration tendency of Ca^{2+} ions changes dramatically with the pulse energy. When the pulse energy is fixed at 2 μJ [Fig. 2(a)], the relative concentration of Ca^{2+} ions increases at the focal point, which is opposite to the results previously obtained at similar laser conditions (800 nm, 250 kHz)[2,22,23]. Then, the pulse energy was increased to 2.72 μJ [Fig. 2(b)]. The relative concentration of Ca^{2+} ions decreases in the central area and increases in the periphery of focal region, forming a ring-shaped enrichment zone. This result is in agreement with previous observations in other glass systems[2,22,23]. It is noted that the distribution of Ca^{2+} ions in Fig. 2(a) is nearly opposite to the one in Fig. 2(b), indicating that the pulse energy is a crucial factor in laser-induced element migration. When the pulse energy reaches 3.12 μJ, it is found that the ring-shaped enrichment zone in Fig. 2(c) has a larger diameter than the one in Fig. 2(b). As the pulse energy continues to increase, a more attractive result is observed. In Fig. 2(d), besides the ring-shaped enrichment zone in the periphery of the laser-affected region, another high concentration zone forms at the focal point. The area between the two enrichment zones has a low Ca^{2+} ions content. Compared with the ion distribution at the pulse energy of 2, 2.72, and 3.12 μJ, this ion distribution is more complex. The dramatic change of ion distribution at different pulse energies provides a possibility that laser-induced micro-modification of element distribution in glass systems can be controlled precisely.

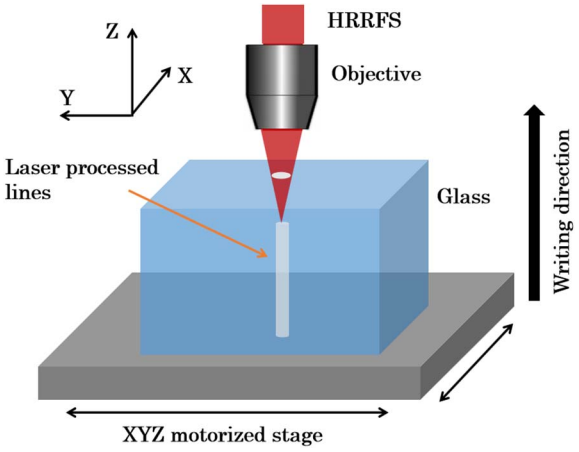

Fig. 1. Experimental scheme of laser processing lines along the *Z* axis inside the oxyfluoride glass.

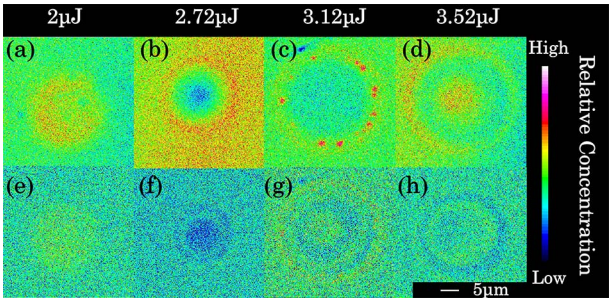

Fig. 2. EPMA mapping showing the distribution of (a)–(d) Ca^{2+} and (e)–(h) Yb^{3+} in the glass with different pulse energies. (a), (e) 2 μJ, (b), (f) 2.72 μJ, (c), (g) 3.12 μJ, (d), (h) 3.52 μJ.

To explore the relationship between the micro-elemental distribution and micro-fluorescence properties, we added Yb^{3+} ions into the sample. Generally, as the network modifier, the distribution of Yb^{3+} ions shows a similar variation tendency with Ca^{2+} ions. However, some unexpected phenomena have been observed. When the pulse energy is 2.72 μJ, the relative concentration of Yb^{3+} ions decreases at the focal point and increases in the periphery, forming two ring-shaped enrichment zones at the periphery of the laser irradiated area [Fig. 2(f)]. It is noted that the distribution of Ca^{2+} ions at this pulse energy only has one ring-shaped enrichment zone. When the pulse energy increases to 3.12 μJ, the distribution of Yb^{3+} ions is no longer similar to the distribution of Ca^{2+} ions at the same pulse energy. Besides the two ring-shaped enrichment zones, another high concentration zone forms at the focal point [Fig. 2(g)]. We noticed that this distribution of Yb^{3+} ions is more similar to the distribution of Ca^{2+} ions

at higher pulse energy [Fig. 2(d)]. If the pulse energy increases continuously (up to 3.52 μJ), both the central enrichment zone and the ring-shaped enrichment zones become larger [Fig. 2(h)].

The distribution of network former Si^{4+} ions was also investigated (Fig. 3). From the EPMA mapping, it can be found that the relative concentration of Si^{4+} ions slightly decreases in the central area at the pulse energy of 2 μJ [Fig. 3(a)], indicating that Si^{4+} ions migrate from the focal point to the periphery of the laser-affected zone. However, as the pulse energy increases, the migration of Si^{4+} ions shows an opposite tendency [Figs. 3(b), 3(c), and 3(d)]. Although the change in the distribution of Si^{4+} ions is less obvious than that of Ca^{2+} and Yb^{3+} ions, the different distributions of Si^{4+} ions at lower and higher energy are still meaningful. Moreover, it is worth noticing that the migration tendencies of Si^{4+} and Ca^{2+} always remain opposite, which are in accordance with the previous studies[2,22,23].

When an HRRFS is focused inside a glass sample, the temperature at the focal point can reach higher than several thousand K (Kelvin) because of the heat accumulation, which leads to localized heating. The subsequent thermal diffusion process will result in sharp temperature and pressure gradients, which drive diffusion of ions in the laser-affected region[2,16]. The chemical diffusion coefficient of elements can be expressed by the equation

$$D = D_0 \exp(-Q/RT), \tag{1}$$

where Q is the activation energy, R is the gas constant, and T is the local temperature[2,32]. Previous studies have proven that glass network modifying ions will migrate to the periphery of the laser focal region due to their higher diffusion coefficient, while glass network forming ions migrate to the central area, filling the vacancies resulted from migration of other ions, since they have a stronger binding energy with oxygen or fluorine than the network modifying ions. However, in the present study, the migration of ions does not follow such principles as stated above, indicating that the elemental migration mechanism is more complex than previously thought. It is probable that some influences besides the temperature and pressure gradients take place in laser-induced element migration.

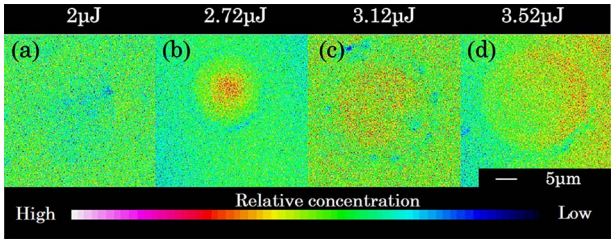

Fig. 3. EPMA mapping showing the distribution of Si^{4+} in the glass with different pulse energies. (a) 2 μJ, (b) 2.72 μJ, (c) 3.12 μJ, (d) 3.52 μJ.

Actually, numerous interesting phenomena may take place in the affected zone of HRRFS, for instance, laser-induced crystallization in glass[33]. At the focal point of an HRRFS, the power density is high enough to bring about the nonlinear absorption, resulting in the generation of high-density electron plasma. Subsequently, the excess energy releases from the plasma into the surrounding media, heating it up. If the glass is heated to the specific temperature and holds for some time, the crystalline phase will precipitate in the glass. Laser-induced space-selective precipitation of crystals has been observed in many glass systems, such as silicate glasses[33] and oxyfluoride glass[34]. Aluminosilicate-based CaF_2–Al_2O_3–SiO_2 oxyfluoride glasses are considered to be the most frequently used glass system for the preparation of glass ceramics with CaF_2 nanocrystals[34]. It has been reported that CaF_2 nanocrystals can be precipitated in SiO_2–Al_2O_3–CaF_2–YbF_3–TbF_3 glass[35], which is the same glass system as we used in our experiment. Therefore, it is reasonable to assume that CaF_2 crystallization may happen in the present experiment.

In principle, the crystallization of glass takes two steps: nucleation and crystal growth[36]. Firstly, nucleation occurs in the region where the temperature is lower than the crystallization temperature. Then, the growth of crystal begins. Since the temperature is the highest at the laser focal point and decreases from the center to the outside, the nucleation usually takes place at a certain distance from the focal point, and the crystal grows toward the inside. Previous studies proposed that the nucleation and crystal growth process may attract the component element of crystals to the crystallization region[36], providing a driving force for element migration. Moreover, it is proved that Yb^{3+} ions can be incorporated into CaF_2 nanocrystals through crystallization[35].

We put forward a tentative explanation on the abnormal element migration in our experiment, including the temperature and pressure gradients, the attraction of CaF_2 crystallization, and the incorporation of Yb^{3+} ions caused by crystallization.

For Ca^{2+} ions, when pulse energy is low (2 μJ), the temperature near the laser focal point is just located in the range that is suitable for crystallization. CaF_2 crystallization takes place in the center of the laser-affected zone. As a component element for CaF_2 crystal, Ca^{2+} ions could be attracted and diffused towards the central area. Meanwhile, the influence of temperature and pressure gradients is limited by the low pulse energy. In this stage, the attraction of CaF_2 crystallization dominates. Ca^{2+} ions show relatively high concentration in the focal region [Fig. 2(a)]. As the pulse energy increases, the temperature near the laser focal point rises. The central area is no longer the right place for crystallization. Nucleation takes place at a certain distance from the focal point, and the CaF_2 crystal grows toward the inside, forming a ring-shaped crystallization area[33]. Ca^{2+} ions could be attracted to the new crystallization region away from the center. Simultaneously, heat accumulation at the laser focal point becomes much more intense that results in sharp temperature and

pressure gradients, driving the Ca^{2+} ions to migrate outward. In this stage, the attraction of CaF_2 crystallization and temperature and pressure gradients work together, driving Ca^{2+} ions to migrate to the periphery of the laser-affected zone [Fig. 2(b)]. The higher pulse power not only leads to a larger diameter of the crystallization circle, but also gives rise to sharper temperature and pressure gradients. All of these result in a larger ring-shaped enrichment zone of Ca^{2+} ions [Figs. 2(c) and 2(d)] compared with the one in Fig. 2(b). When the pulse energy rises to a certain value (3.52 μJ) due to the accumulation of a large amount of heat, the temperature in the laser-affected zone cannot rapidly drop to the solidification point of glass after laser irradiation. This keeps the glass in a molten state for a short time after laser irradiation, and some Ca^{2+} ions may migrate back to the central area under the influence of the concentration gradient. Moreover, during the relatively lengthy cooling process, the temperature of the focal region may get into the temperature range of nucleation and crystallization. It is possible for CaF_2 crystallization to take place in the central area a short time after laser irradiation. This may result in a central enrichment zone of Ca^{2+} ions in the laser-affected region, as presented in Fig. 2(d).

The redistribution of Yb^{3+} ions is generally similar with Ca^{2+} ions. When pulse energy is low (2 μJ), CaF_2 crystallization takes place in the center of the irradiated region, incorporating some Yb^{3+} ions into the CaF_2 crystal. Therefore, Yb^{3+} ions show relatively high concentration in the focal region [Fig. 2(e)]. As the pulse energy increases, Ca^{2+} ions migrate to the periphery of the laser-affected zone. The crystallization region of CaF_2 changes from the central point to a circle around the focal point. Some Yb^{3+} ions are incorporated into the CaF_2 crystal circle, forming a ring-shaped enrichment zone, which is presented as the outer ring in Fig. 2(f). Meanwhile, temperature and pressure gradients drive the Yb^{3+} ions to migrate outward, forming another ring-shaped enrichment zone, which is presented as the inner ring in Fig. 2(f). As the ratio of charge/ion radius for Yb^{3+} is larger than that of Ca^{2+}, which may result in poorer mobility of Yb^{3+} than that of Ca^{2+} to pass through the glass network during irradiation, it can be inferred that Yb^{3+} ions have a lower migration speed away from the focal center compared with Ca^{2+} ions. Considering the difference in migration speed, it is reasonable that the diameter of the ring-shaped enrichment zone of Yb^{3+} ions in Fig. 2(f) is smaller than that of Ca^{2+} ions in Fig. 2(b). Comparing the distribution of Yb^{3+} ions in Figs. 2(f), 2(g), and 2(h), it is also observed that both the inner and outer rings become larger as the pulse energy increases. Two factors may lead to this phenomenon. Firstly, the higher pulse power leads to a larger diameter of the CaF_2 crystallization circle at the periphery of the laser-affected zone. Yb^{3+} ions are incorporated into the CaF_2 crystal and form a larger outer ring-shaped enrichment zone. Secondly, the higher pulse power also leads to sharper temperature and pressure gradients, which pull the Yb^{3+} ions outward to form a larger inner ring-shaped enrichment zone of Yb^{3+} ions. Besides the ring-shaped enrichment zones, the high concentration areas in the central part of Figs. 2(g) and 2(h) are remarkable. We pose a hypothesis to explain this phenomenon that occurs at high pulse energy. Firstly, some Yb^{3+} ions may diffuse back to the central area under the influence of the concentration gradient, since the intense accumulation of heat keeps the glass in a molten state for a short time after the high-power laser irradiation. Secondly, the temperature in the laser focal zone at high pulse energy may be suitable for the crystallization of YbF_3. The nucleation and crystallization of YbF_3 attract the surrounding Yb^{3+} ions, driving them to migrate inward. Thus, central enrichment zones of Yb^{3+} ions are formed in the laser-affected region. However, further investigations are needed to prove this hypothesis.

The distribution of Si^{4+} ions shows an opposite tendency with Ca^{2+} ions at different pulse energies. Since the network formers have a stronger binding energy with oxygen than the network modifiers, the diffusion coefficient of the network former Si^{4+} ions is generally much smaller than that of the modifier Ca^{2+} ions. Si^{4+} ions are apt to migrate slowly, filling the vacancies resulted from migration of other ions for change balance[2]. Thus, when pulse energy is low (2 μJ), Ca^{2+} ions diffuse towards the focal center and show relatively high concentration in the focal region. Simultaneously, a few Si^{4+} ions migrate outward to fill the vacancies around the central enrichment zone of Ca^{2+} ions, causing a slight decrease of Si^{4+} ions at the focal point [Fig. 3(a)]. As the pulse energy increases, Ca^{2+} ions diffuse away from the center, leaving a lot of vacancies in the central area. Si^{4+} ions migrate inward, forming a central enrichment zone in the center of the laser-affected area [Figs. 3(b), 3(c), and 3(d)].

In order to investigate micro-property changes of the glass resulted from the element redistribution, the fluorescence intensities of Yb^{3+} at pulse energies of 2.72 and 3.12 μJ were measured. Confocal fluorescence spectra were acquired at different positions (a–l) of the laser-affected zone under 785 nm laser irradiation (Fig. 4). The infrared emission at 975 nm [Fig. 4(b)] in the glass can be attributed to the $^2F_{5/2}(Yb^{3+}) \rightarrow {}^2F_{7/2}(Yb^{3+})$ transitions of Yb^{3+}. Representative points in which the relative concentration of Yb^{3+} ions is extremely high or low were selected and presented clearly in Figs. 4(a) and 4(c). The fluorescence intensities of these points are illustrated in Figs. 4(d) and 4(e). Through these figures [Figs. 4(a), 4(c), 4(d), and 4(e)], it is easy to associate the change in fluorescence intensities with the element redistribution induced by laser irradiation. Although the micro-fluorescence intensity of Yb^{3+} is affected by many factors, it is clear that the controllable element distribution plays a significant role in changing the micro-fluorescence property of glass. It should be pointed out that not only the micro-fluorescence property can be changed by laser-induced element migration. This technique can be used to modify many other micro-property of materials, like refractive index. More applications will be developed based

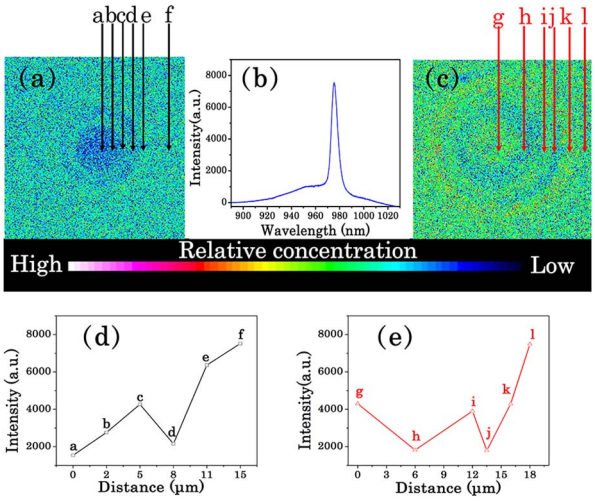

Fig. 4. (a), (c) EPMA mapping showing the distribution of Yb^{3+} ions in the glass with different pulse energies. (b) Confocal fluorescence spectrum obtained with a 785 nm laser as the excitation source. (d), (e) Different luminescence intensities at 975 nm as a function of distance. The special points a–l are presented clearly in (a) and (c).

on laser-induced element migration, such as micro-shaped waveguides.

In the present work, we have reported on abnormal element redistribution in oxyfluoride glasses induced by a 250 kHz fs laser. The elemental distribution analyses demonstrate complex migration behaviors of Ca^{2+}, Yb^{3+}, and Si^{4+} ions at different pulse energies. We attribute these complex migration behaviors to the influences of temperature and pressure gradients, the attraction of CaF_2 crystallization, and the incorporation of Yb^{3+} ions caused by crystallization. The change in fluorescence intensities caused by element redistribution is also investigated. This study opens a new way to understand the mechanism of fs-laser-induced element redistribution. It is proved that a single fs laser beam can realize diversiform micro-modification of elemental redistribution, which is crucial for improving the micro-property of materials. We also believe this result will help in resolving other irregular phenomena in the area of modification of materials with ultrafast lasers, such as abnormal refractive index changes in some glasses. These findings in the present work may be helpful for fabricating microstructures that may find promising applications in integrated optics, such as nonlinear optical waveguides.

References

1. R. R. Gattass and E. Mazur, Nat. Photon. **2**, 219 (2008).
2. D. Tan, K. N. Sharafudeen, Y. Yue, and J. Qiu, Prog. Mater. Sci. **76**, 154 (2016).
3. X. Liu, J. Zhou, S. Zhou, Y. Yue, and J. Qiu, Prog. Mater. Sci. **97**, 38 (2018).
4. J. Qiu, K. Miura, and K. Hirao, J. Non-Cryst. Solids **354**, 1100 (2008).
5. D. Chu, X. Sun, Y. Hu, X. Dong, K. Yin, Z. Luo, J. Zhou, C. Wang, and J. Duan, Chin. Opt. Lett. **15**, 071403 (2017).
6. X. Dong, Z. Xie, Y. Song, K. Yin, D. Chu, and J. Duan, Chin. Opt. Lett. **15**, 090602 (2017).
7. J. Thomas, M. Heinrich, J. Burghoff, and S. Nolte, Appl. Phys. Lett. **91**, 151108 (2007).
8. S. Kawata, H. B. Sun, T. Tanaka, and K. Takada, Nature **412**, 697 (2001).
9. Y. Shimotsuma, P. G. Kazansky, J. Qiu, and K. Hirao, Phys. Rev. Lett. **91**, 247405 (2003).
10. S. Juodkazis, K. Nishimura, H. Misawa, T. Ebisui, R. Waki, S. Matsuo, and T. Okada, Adv. Mater. **18**, 1361 (2006).
11. K. Miura, J. Qiu, H. Inouye, and T. Mitsuyu, Appl. Phys. Lett. **71**, 3329 (1997).
12. J. Qiu, K. Miura, T. Suzuki, and T. Mitsuyu, Appl. Phys. Lett. **74**, 10 (1999).
13. J. Qiu, C. Zhu, T. Nakaya, J. Si, K. Kojima, F. Ogura, and K. Hirao, Appl. Phys. Lett. **79**, 3567 (2001).
14. J. Qiu, X. Jiang, C. Zhu, M. Shirai, J. Si, N. Jiang, and K. Hirao, Angew. Chem. Int. Edit. **43**, 2230 (2004).
15. J. Qiu, M. Shirai, T. Nakaya, J. Si, X. Jiang, C. Zhu, and K. Hirao, Appl. Phys. Lett. **81**, 3040 (2002).
16. Y. Liu, B. Zhu, L. Wang, J. Qiu, Y. Dai, and H. Ma, Appl. Phys. Lett. **92**, 121113 (2008).
17. K. M. Davis, K. Miura, N. Sugimoto, and K. Hirao, Opt. Lett. **21**, 1729 (1996).
18. A. M. Streltsov and N. F. Borrelli, Opt. Lett. **26**, 42 (2001).
19. K. Miura, J. Qiu, S. Fujiwara, S. Sakaguchi, and K. Hirao, Appl. Phys. Lett. **80**, 2263 (2002).
20. Y. Liao and Y. Cheng, Micromachines **5**, 1106 (2014).
21. Y. Cheng, Micromachines **8**, 59 (2017).
22. Y. Teng, J. Zhou, G. Lin, J. Hua, H. Zeng, S. Zhou, and J. Qiu, J. Non-Cryst. Solids **358**, 1185 (2012).
23. Y. Liu, M. Shimizu, B. Zhu, Y. Dai, B. Qian, J. Qiu, Y. Shimotsuma, K. Miura, and K. Hirao, Opt. Lett. **34**, 136 (2009).
24. X. Wang, M. Sakakura, Y. Liu, J. Qiu, Y. Shimotsuma, K. Hirao, and K. Miura, Chem. Phys. Lett. **511**, 266 (2011).
25. Z. Tu, Y. Teng, J. Zhou, S. Zhou, H. Zeng, and J. Qiu, J. Raman Spectrosc. **44**, 307 (2013).
26. F. Luo, J. Song, X. Hu, H. Sun, G. Lin, H. Pan, Y. Cheng, L. Liu, J. Qiu, Q. Zhao, and Z. Xu, Opt. Lett. **36**, 2125 (2011).
27. S. Zhou, N. Jiang, K. Miura, S. Tanabe, M. Shimizu, M. Sakakura, Y. Shimotsuma, M. Nishi, J. Qiu, and K. Hirao, J. Am. Chem. Soc. **132**, 17945 (2010).
28. M. Sakakura, T. Kurita, M. Shimizu, K. Yoshimura, Y. Shimotsuma, N. Fukuda, K. Hirao, and K. Miura, Opt. Lett. **38**, 4939 (2013).
29. M. Shimizu, M. Sakakura, S. Kanehira, M. Nishi, Y. Shimotsuma, K. Hirao, and K. Miura, Opt. Lett. **36**, 2161 (2011).
30. M. Shimizu, K. Miura, N. Yasuda, M. Sakakura, S. Kanehira, M. Nishi, Y. Shimotsuma, and K. Hirao, in *MRS Online Proceedings Library Archive* (2009), p. 1230.
31. F. Zhang, Z. Tu, X. Du, H. Zhang, and J. Qiu, Mater. Lett. **137**, 92 (2014).
32. X. Zhang, X. He, Q. Liu, B. Poumellec, M. Lancry, and F. Brisset, J. Alloy. Compd. **727**, 444 (2017).
33. Y. Yonesaki, K. Miura, R. Araki, K. Fujita, and K. Hirao, J. Non-Cryst. Solids **351**, 885 (2005).
34. K. Shinozaki, A. Noji, T. Honma, and T. Komatsu, J. Fluorine. Chem. **145**, 81 (2013).
35. S. Ye, B. Zhu, J. Chen, J. Luo, and J. Qiu, Appl. Phys. Lett. **92**, 141112 (2008).
36. T. Komatsu, J. Non-Cryst. Solids. **428**, 156 (2015).